Available online at www.sciencedirect.com
ScienceDirect
Corrosion Science 49 (2007) 231–239
CORROSION SCIENCE
www.elsevier.com/locate/corsci

# Single particle impact experiments for studying particle induced flow corrosion

Achim Walter Hassel *, Andrew J. Smith

*Max-Planck-Institut für Eisenforschung, Max-Planck-Str. 1, D-40237 Düsseldorf, Germany*

Available online 7 July 2006

**Abstract**

An experimental set-up for the investigation of particle induced flow corrosion is described. It allows high speed monitoring of the repassivation current transient resulting from the impingement of a single particle. High purity aluminium microelectrodes with a diameter of 125 μm were used as targets in a neutral acetate buffer. Zirconia spheres of similar diameter were impinged at a flow rate of 7 m $s^{-1}$. After an activation period of about 6 μs the current reaches a peak current of 10 μA. The current returns to its initial base line within one millisecond. Subsequent ex situ investigation of the samples in a SEM allows linking the detected surface destruction to its current transient. A crater of some 20 μm diameter is observed that shows a nanoscopic substructure resulting from the nanostructure of the particle. Part of the repassivation charge must be determined by an extrapolation of the high field oxide growth. A comparison of the consumed charge to the microscopic observations gives insights into the destruction mechanisms.


*Keywords:* A. Aluminium; B. Erosion; B. SEM; C. Repassivation; C. Tribocorrosion

## 1. Introduction

The disastrous effect of tribocorrosion results from a combined mechanical attack and an aggressive environment. Due to a synergistic effect the material loss can be much larger than the sum of erosion and corrosion [1]. The most common experimental approaches

* Corresponding author. Tel.: +49 211 6792 464; fax: +49 211 6792 218.
*E-mail address:* hassel@elchem.de (A.W. Hassel).

0010-938X/$ - see front matter © 2006 Elsevier Ltd. All rights reserved.
doi:10.1016/j.corsci.2006.05.021

were reviewed by Landolt et al. [1,2]. The tribological contact can be of various natures; sliding, fretting, rolling or impingement. Also the effect of two body erosion–corrosion and three body erosion–corrosion – with an added abrasive – are discussed.

Particle induced flow corrosion is a type of erosion corrosion which can be observed in cooling water circuits or on marine propellers. Studying this mechanism is possible by a slurry jet that sprays a mixture of a liquid phase and a solid phase against the material of interest [3]. This type of material destruction is always accompanied by an increase of the roughness [4] and a surface hardening [5]. The mechanical and electrochemical interaction under these conditions was studied by Neville and Hu [6]. A more general description was given by Stack and Pungwiwat [7] focusing on a discussion of the synergistic effect. Soon the interest in the effect and interaction of single impingement was discussed and experimentally addressed. Sasaki and Burstein refined the method to detect discrete transients from single impacts in the same experiment [8]. On stainless steel they observed a threshold impact energy required to cause the rupture of the passive film [9]. A similar approach was used to study cavitation corrosion [10].

In this work the emphasis was set on developing an experiment that allowed studying the current transients resulting from the impact of one single particle and to correlate this very impact to the subsequent ex situ investigations – such as SEM, AFM – of the resulting wear. The idea behind this work was to reduce the number of particles and decrease the size of the working electrode in order to reduce the impact probability. In this manner multiple impacts to the same sample were highly improbable.

## 2. Experimental

### 2.1. Electrodes

High purity aluminium 99.999% wires (Goodfellow, diameter 125 μm) were used to prepare μ-disc electrodes. Glass capillaries were pulled by means of a capillary puller (Narishige) and ground to a diameter of 130 μm. Subsequently liquid polymer was drawn into the capillary using a vacuum pump and the wire was inserted. After hardening of the polymer the microelectrode was mounted in a mechanically stable second glass capillary with an attached gold counter electrode. After grinding, a 125 μm μ-disc electrode resulted, as shown in Fig. 1. A $Hg/Hg_2^I(OOCCH_3)_2$ reference electrode was connected via a Lugin capillary (Fig. 1) [11]. The potential defining step of the mercury acetate electrode results from the electrolyte itself, thus it has some advantages:

- fast response;
- simple application;
- no diaphragm; and
- no diffusion potentials.

### 2.2. Chemicals

All solutions were prepared from p.a. grade chemicals and high purity water (Millipore filter system). A 0.1 mol $dm^{-3}$ acetate buffer of pH 6.0 was used for all experiments yielding a corrosion minimum and a low background current [12].

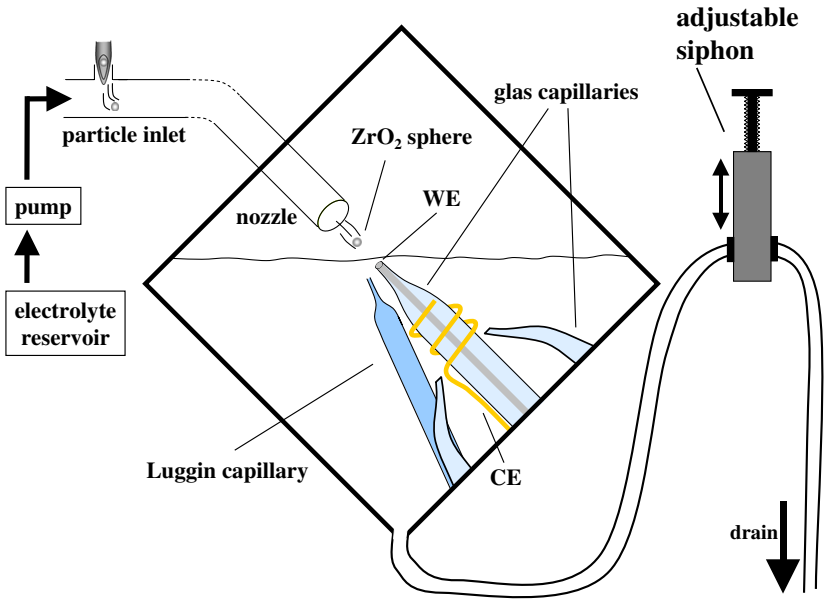


Fig. 1. Schematic of the Slurry jet impingement system. The slurry ejecting nozzle faces the immersed working electrode (WE) and can be adjusted by a *xy*-stage. Counter and reference electrode are in close vicinity of the WE. The adjustable siphon allows precise control of the electrolyte level in the chamber.

### 2.3. Slurry jet

The Slurry jet consists of an acrylic, cube shaped chamber set on a corner (Fig. 1). The nozzle (made from a Pasteur pipette (diameter = 1 mm)) and the sample are mounted to facing walls of the chamber. A high performance pump with an extreme acceleration of 20,000 revolutions $s^{-2}$ reaches its maximum speed within 3 ms to allow instant spraying.

The lower tip of the cube acts as a drain. By mounting the nozzle to a *xy*-stage it is possible to aim the slurry jet at the sample.

In order to introduce a well defined number of spheres into the system a particle inlet was constructed from Plexiglas with a main channel for the electrolyte and a small perpendicular loading channel through which the spheres were introduced to the system using a hypodermic needle. Prior to loading, the spheres were counted under a microscope. Unlike other set-ups described [6–8] neither electrolyte nor impacting particles were recycled.

### 2.4. Particles

The abrasive particles used in these experiments were zirconia spheres (Fuji, Japan). For size distribution refer to Section 3.

### 2.5. Electronics

A crucial point in the measurement of current transients during slurry jet impingement is the data acquisition since the transients contain a lot of information about the

mechanism [13]. Since the time of impact of the particle is not exactly known but the transient of interest shall be recorded with sufficient resolution in time it is desirable to constantly use a high data acquisition rate. Consequently a new set-up was constructed that is able to measure current transients continuously at a rate of up to 20 MHz which is schematically shown in Fig. 2.

This system consists of a fast current to voltage converter (FACCON) with a band width of about 5 MHz. The combination of a small measurement resistor with a near sample impedance conversion and a post amplification of the signal allowed the measurement of currents in the 100 nA to 10 μA-range at rates of 1 MHz. This current proportional voltage and the electrode potential itself are then converted by the analog to digital converter (ADC). This ADC possesses four independent 12 bit 20 MHz converters which are able to convert continuously at this rate. At 1 MHz in 2 channel mode (current and potential) each second 4 MByte are produced corresponding to a data rate of 32 Mbit $s^{-1}$. To establish a quasi real time system that is capable of measuring this data continuously it must be guaranteed that an overflow never occurs during the entire experiment. The architecture used here consists of four data buffers with increasing size and decreasing speed. The first memory is a fast static dual line FIFO (first in first out). The data is written into FIFO1 until it is full. Then writing from the ADC continues into the second FIFO and vice versa. Simultaneously the data from FIFO1 is transferred to a larger second level cache 512 kByte in size that is operating in LRU mode (least recently used). Thus the switching between write and read modus is minimized and the data can be transferred in the burst mode with a simple incremental memory addressing. The data is transferred to the system RAM and finally stored on two SATA hard discs (RAPTOR Western

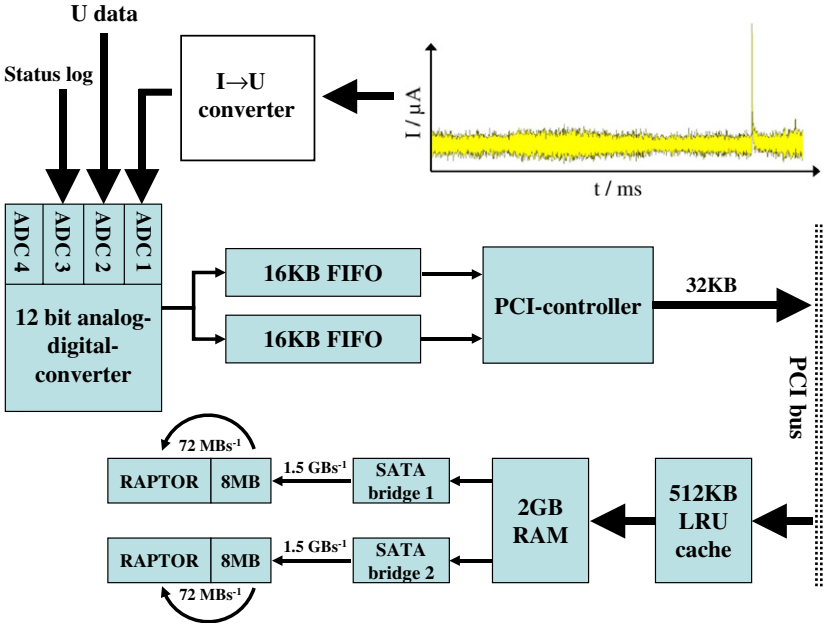


Fig. 2. Simplified chart of the high speed data acquisition and storage system used. Detailed description is given in the text.

Digital, 10,000 rpm) each being connected to its own controller. This architecture is used to optimise the performance of the mass storage device since the data is simultaneously transferred to both hard discs to allow maximum performance. With the maximum buffer to host transfer speed of 1.5 Gbit $s^{-1}$ and a sustained buffer to disk transfer speed of 72 Mbit $s^{-1}$ each, no buffer overflows resulting in delays were observed in the experiments.

## 3. Results and discussion

The particle size and thus the mass are crucial factors. For a given velocity $v$, the kinetic energy $E_{kin}$ of a particle scales linearly with its mass $m$:

$$E_{kin} = 1/2mv^2 = 2\pi/3\rho r^3 v^2. \quad (1)$$

The mass of a single particle is hard to determine. Hence, an indirect way of determining the mass distribution was chosen. The density of the spheres is known to be 5700 kg $m^{-3}$. To determine the diameter a conductive and gluey carbon pad was tapped onto the spheres in order to form a monolayer. It was then investigated in a SEM as seen in the left inset in Fig. 3. 12297 particles were analysed by an image analysis software to determine the diameter of each single particle. All spheres were classified and the abundance of the sphere diameter was plotted in the histogram in Fig. 3. For comparison the black bell curve shows the Gaussian fit of the data. Even though the distribution is not exactly gaussian the mode was determined to be 117 μm and the $2\sigma$ range (68%) lies between 112 and 122 μm. The sphere impulse as calculated for a jet velocity of 7 m $s^{-1}$ was plotted in Fig. 3 as the upper abscissa. The units are not equidistant since the impulse scales with the third power of the diameter.

The insets on the right side in Fig. 3 show close up views of the spheres which will be discussed later.

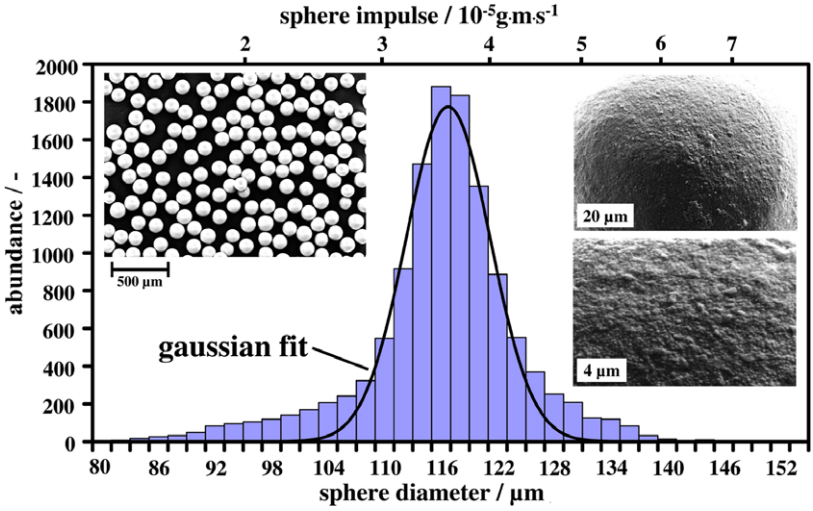


Fig. 3. Distribution of abrasive particle sizes. The upper $x$-axis shows the sphere impulse calculated for a speed of 7 m $s^{-1}$. The most abundant diameter is 117 μm. The insets show SEM-micrographs of the abrasive particles at different magnifications.

In order to obtain an estimate of the probability of impact for a given μ-disc sample diameter targeting, experiments were performed. The experiment consisted of introducing a defined number of abrasive particles into the system and shooting them at a macroscopic aluminium sample. Geometrically separated craters were found within the radius of the nozzle. All impacts were circular having the same average size. This proves that the impact angle remains 90° and the *xy*-stage can be used to tune the impact probability.

An aluminium microelectrode with a diameter of 125 μm was mounted from the lower side into the cube as shown in Fig. 1. The siphon was adjusted in a way that the electrolyte level just covered the electrode of interest, allowing potentiostatic control of the sample and a minimized retardation of the jet when entering the solution.

The electrode was polarized potentiostatically at 2 V HESS (hydrogen electrode same solution) to form the initial oxide. With a film formation factor of 1.6 nm $V^{-1}$ and an oxide formation potential of −1.6 V HESS an initial oxide film thickness of 5.8 nm results [14]. Throughout the entire following experiment the sample was held potentiostatically at this potential. For the impingement experiment itself some 20 spheres were loaded into the main channel using a hypodermic needle. After loading the particles the system was sealed and the experiment was started. In Fig. 4a an excerpt of the current transient is shown. This excerpt contains the only current peak observed in the entire transient resulting from the impact of a single particle. The diameter of the electrode is almost identical with that of the particles. Hence, for geometrical reasons, it is impossible for two particles to hit the surface simultaneously. A first characterisation of the recorded current transient is possible by evaluating its key parameters such as peak current $I_{max}$, time of peak current $t_0$, current rise time $t_{rise}$, repassivation time $t_{recover}$, and background current $I_{back}$.

The time axis was normalised to the time of peak current $t_0$. The peak current in this experiment was 10 μA. The increase in current is rapid; the rise time is only 6 μs before the current reaches its maximum. The current then decreases to its initial background level

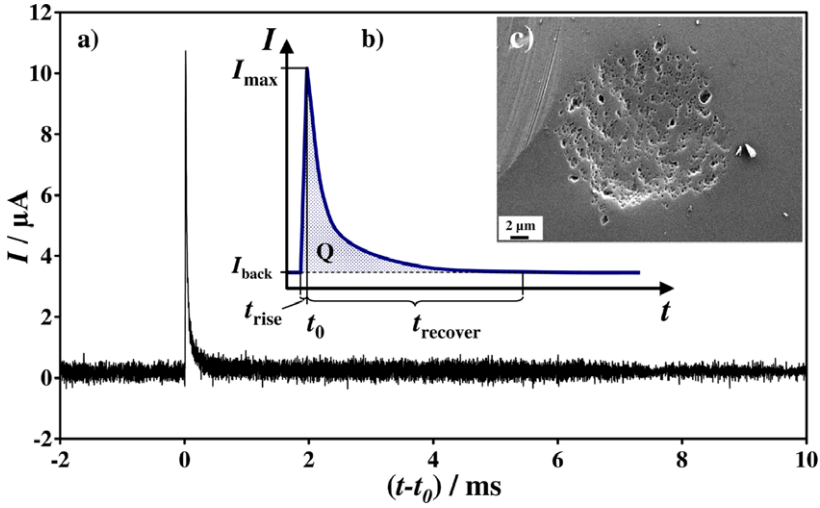


Fig. 4. (a) Current transient normalised to the time of peak current $t_0$. (b) Schematic current transient with all characteristic parts marked. (c) SEM-micrograph of the resulting crater.

within some 300 μs. The transient shows an exponential decay, typical for a self inhibiting process such as repassivation.

The electrode on which the transient in Fig. 4a was recorded was removed from the slurry jet, thoroughly rinsed with water, dried and investigated further in a SEM. A microscopic view of the impact crater is shown in Fig. 4c. The diameter of the impact crater is approximately 20 μm with a clear fine structure and a feature size in the upper nanometer range. The size and appearance of these nanoscopic indents obviously fits to the nanoscopic substructure of the impacting particles as seen in the upper and lower insets on the right side in Fig. 3. The most elevated surface feature of the particle would correlate to the deepest nanoscopic impact in Fig. 4c. The overall shape of the sphere causes the crater which is seen in Fig. 4c. The fact that the crater in Fig. 4c has a more or less round shape and no significant scratches caused by the nanoscopic protrusions indicates that the spheres impulse is transferred to the electrode immediately and the sphere most likely loses its whole energy. Removal of the particle from the sample surface is probably caused by the electrolyte jet.

The time for the current to return to the background level $t_{recover}$ in Fig. 4a is approximately 300 μs. From experiments with macroscopic samples it is known that the repassivation takes much longer. Depending on the solution which determines the stationary corrosion current this may take 1 s in aggressive solutions up to a few hundred seconds in a neutral buffer [13]. In an attempt to estimate the "true" charge the current transient of Fig. 4a was plotted again in a double logarithmic representation in Fig. 5. A straight line was fitted to the data between $10^{-4.5}$ s and $10^{-3.5}$ s which is dominated by the high field oxide growth of the freshly bared surface. This line has a slope near unity and is exactly described by the equation given as an inset in Fig. 5. Assuming that the repassivation of the impinged area continues independently from the simultaneous stationary corrosion of the rest of the area which causes a much higher current, the current would decay on the −1 slope for 100 s. For each decade in time – indicated by the vertical lines – the

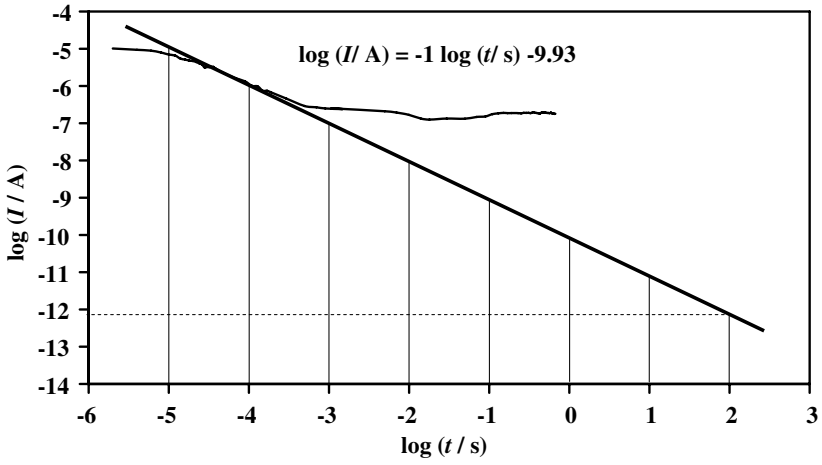


Fig. 5. Double logarithmic plot of the data from Fig. 4a. The equation describes the fit applied to the high field part of the plot. The intercept of this fit with the time value of 100 s yields an approximation of the repassivation current.

same increment of charge is consumed. This means that only some 30% of the repassivation charge would be found if the integration was performed within $t_{recover}$. The most appropriate way to determine the charge consumed seems to be a numerical integration for the first two segments and integration over the extrapolation line for the last six segments. In this way a charge of 1.89 nC was determined. Under the potentiostatic conditions in this experiment the film thickness remains constant. Therefore – in the absence of side reactions – the charge consumed is equivalent to a well defined volume of oxide [13]. Thus the repassivated surface area (16.1 $\mu m^2$) can be derived from the charge.

When compared to the crater shown in Fig. 4c it becomes obvious that only 5.63% of the surface is bared during the impingement. Strictly speaking the increase in surface area resulting from the transformation of a plane to a bowl bottom shape caused by the impacting particle would contribute 0.66% of the charge. Thus approximately 5% of the surface was bared during impingement.

## 4. Conclusions

An experimental set-up for the investigation of particle induced flow corrosion is described. It allows a high speed monitoring of repassivation current transients resulting from the impingement of a single particle. The activation of the surface requires approximately 6 μs. After the peak current an exponential decay of the current is observed before the current returns to its initial value within 300 μs. Subsequent ex situ investigations by SEM allowed determining the impact crater. It has a diameter of approximately 20 μm and a bowl bottom shape with a nanoscopic substructure resulting from the nanoscopic protrusions of the impacting particle. The increase in surface as compared to the projection of the crater is less than 1% but the bared surface calculated from the charge consumed is some 5% of the crater surface under these potentiostatic conditions. A plausible explanation is a kind of nanopiercing of the surface next to the formation of cracks in the brittle oxide layer.

Under the chemically mild conditions chosen here no significant chemical attack must be considered. Nevertheless the background current of the non impinged area masks most of the charge resulting from the repassivation of the bared surface. This requires that the charge be determined based on the extrapolation of the high field line for the time that is usually required for a repassivation in the electrolyte under investigation.

The advantage of the experimental set-up described here is the clear link between the transient resulting from the impact of a single particle and the possibility to perform investigations on precisely the scar caused by one impinging particle. Future studies should include different materials such as copper and stainless steels in various media of different aggressivity. Moreover physical parameters such as abrasive particle geometry, size and mass should be varied as well as the investigation of the effect of particle velocity and impact angle.

## Acknowledgements

The authors would like to express their sincere thanks to E. Akiyama for assistance in setting up a first version of the slurry jet. We wish to thank J.W. Schultze and M. Schramm from the AGEF e.V. for making available the FACCON. Thanks are due to M. Stratmann, M.M. Lohrengel and G.T. Burstein for helpful discussions.

## References

[1] D. Landolt, S. Mischler, M. Stemp, Electrochim. Acta 46 (2001) 3913–3929.
[2] D. Landolt, S. Mischler, M. Stemp, S. Barril, Wear 256 (2004) 517–524.
[3] J.B. Zu, I.M. Hutchings, G.T. Burstein, Wear 140 (1990) 331–344.
[4] K. Sasaki, G.T. Burstein, Corros. Sci. 38 (1996) 2111–2120.
[5] M. Tennichi, T. Nakagawa, Jpn. Soc. Lubr. Eng. 33 (1988) 839–847.
[6] A. Neville, X. Hu, Wear 251 (2001) 1284–1494.
[7] M.M. Stack, N. Pungwiwat, Wear 256 (2004) 565–576.
[8] G.T. Burstein, K. Sasaki, Electrochim. Acta 46 (2001) 3675–3683.
[9] K. Sasaki, G.T. Burstein, Philos. Mag. Lett. 80 (2000) 489–493.
[10] P.R. Birkin, D.G. Offin, T.G. Leighton, Wear 258 (2005) 623–628.
[11] A.W. Hassel, Elektronische und Ionische Transportprozesse in ultradünnen Ventilmetalloxidschichten, Shaker Verlag, Aachen, 1997, ISBN 3-8265-2981-2, pp. 18–24.
[12] M. Pourbaix, Atlas of Electrochemical Equilibria in Aqueous Solutions, National Association of Corrosion Engineers, Houston, 1974, pp. 168–176.
[13] M.M. Lohrengel, Mater. Sci. Eng. R 11 (1993) 243–294.
[14] J.W. Schultze, A.W. Hassel, in: A.J. Bard, M. Stratmann, M. Stratmann (Eds.), Passivity of Metals Alloys and Semiconductors in Encyclopedia of Electrochemistry, in: M. Stratmann, G.S. Frankel (Eds.), Corrosion and Oxide Films, vol. 4, Wiley-VCH, Weinheim, 2003, pp. 216–270, 188–189.